Isotherm and Kinetic Studies of Malachite Green by NaOH-Activated Carbon Made from Apple Waste

Narayani Balasubramaniam* **and Isana Supiah Yosephine Louise**

Department of Chemistry Education, Universitas Negeri Yogyakarta, Jl. Colombo No. 1, Yogyakarta 55281, Indonesia

* ***Corresponding author:***

tel: +62-81262142748
email: bnarayani.2020@student.uny.ac.id

Received: January 28, 2025
Accepted: March 28, 2025

DOI: 10.22146/ijc.104046

Abstract: *Using textile dyes that seem to reach new heights has caused the waste produced to skyrocket. One is malachite green, which earned its popularity due to its vibrancy. However, the impact of malachite green has proven to be an adversary to the environment, aquaculture, and health. This experiment aims to analyze the removal of malachite green through adsorption by using activated carbon made from apple waste. Some activated carbon underwent activation with NaOH 0.5 M. We sieved these activated carbons into a 100 mesh and used the batch method to test them for optimal conditions. The concentration at equilibrium was analyzed using cyclic voltammetry. The results of these experiments are modeled into isotherm and kinetics models to help describe the adsorption. SEM-EDS, FTIR, and SAA also characterized the adsorbent samples. We found the NaOH-activated carbon to be the most efficient adsorbent, with optimum conditions of 0.3 g, 20 min, and 200 ppm. The adsorption data followed the Dubinin-Radushkevich isotherm and the pseudo second-order kinetics.*

Keywords: *activated carbon; adsorption; apple waste; malachite green*

■ INTRODUCTION

Textile dyes have been increasingly popular in modern times due to their bright colors and versatility compared to natural dyes. Nonetheless, their influence on the environment, particularly the aquatic ecosystem, has been proven to be toxic. The textile industry in Indonesia frequently discharges trash into rivers, resulting in aquatic pollution [1]. This textile dye waste may obstruct sunlight from reaching the water's surface. In addition to the aquatic environment, textile dyes also negatively impact health. These encompass skin and eye irritation, cancer development, and mutation [2]. Consequently, the appropriate handling of textile dyes and compliance with standards is crucial in preventing pollution and undesirable societal effects.

Malachite green is one of the most often utilized textile colors. Malachite Green presents a uniquely vivid hue of green in contrast to other dyes. It dyes wool, silk, skin, and paper. In addition to its role as a coloring agent, malachite green functions as an antibacterial agent, fungicide, bactericide, and pesticide within the aquaculture sector [3-4]. This dye is renowned for its toxicity and has been linked to the stunted growth rate, birth abnormalities, and survivability of fishes [5]. Consequently, the application of malachite green in the aquaculture sector is explicitly prohibited in numerous areas, including Canada, the United States, Europe, and China, with a legal concentration limit of 0.5–100 µg/L [6]. Malachite green poses a risk of groundwater contamination, making it unfit for human consumption. Untreated wastewater containing malachite green mixed with water supplies presents significant risks to human health, including mutagenesis, carcinogenesis, and severe damage to the respiratory system [7]. Nevertheless, nations with less strict regulations, such as Indonesia, would continue to permit the utilization of malachite green.

Various strategies have been employed to mitigate the water quality crisis in Indonesia. The techniques utilized in the treatment of textile wastewater include coagulation [8], electrocoagulation [9], adsorption [10], irradiation [11], photocatalysis [12], ozonation [13], membrane separation [14], and bioremediation [15]. Nonetheless, these approaches are extremely costly and

require complex systems, which limit their application [16]. An inexpensive and relatively simple method for bettering water quality is adsorption.

Adsorption is a method used for liquid waste treatments due to its ability to remove pollutants that need to be removed. Different materials, including activated carbon (AC), were used as adsorbents in the liquid waste treatment. AC is an adsorbent frequently used for waste treatments, gas purification, and catalyst support [17]. AC production would involve dehydration and carbonization of material, followed by physical or chemical activation. Many studies attempt to find alternative materials that could be transformed into AC to suppress costs further. Recently, agricultural wastes, such as peels, seeds, pits, and pulps, have risen to prominence as materials suitable for AC production [18-19]. Several studies have looked at how to make AC from agricultural wastes like rice husks [20], avocado seeds [21], coconut shells [22], sesame shells [23], and cotton stalks [24].

One of the organic materials that could be utilized to obtain AC is apple waste. Apple has established itself as a widely favored commodity globally, with production surpassing 97.00 million tons in 2023. Asia is the major global producer of apples, accounting for approximately 60.00% of worldwide apple production. This trend is evident in Indonesia, in which per capita apple consumption reached 79.21 kg in 2021 [25]. Therefore, the number of apple peels and pulps produced yearly would also be extremely high, intensifying the existing issue of food waste in Indonesia.

Chemical activations are frequently employed to produce ACs that exhibit larger specific surface areas and enhanced porosity [24]. The common reagents utilized for the activation of carbons include NaOH, KOH, H_3PO_4, $ZnCl_2$, HNO_3, and K_2CO_3. Several research studies have been done using apple waste as the source material for AC in the past. Suarez-Garcia [26] made AC from apple peels and used H_3PO_4 as the activator. Ramdane et al. [27] once observed ACs made from apple waste, which involved physical and microwave activation. Currently, there appears to be a lack of studies exploring the use of NaOH as an activator for carbon sourced from apple waste, even though it is recognized as a widely used and low-cost reagent for activation. Other studies have demonstrated that NaOH serves as an excellent activator, facilitating the formation of micropores and mesopores, enlarging its surface area, and improving its adsorption capacity, which is favorable for adsorption [28-30].

The purpose of this study is to find out how well-AC made from apple waste works as an adsorbent, especially when activated using 0.5 M NaOH. We examined the adsorption conditions, including the mass of the adsorbent, the duration of adsorption, and the initial concentration of malachite green, to identify the optimal parameters for the adsorption process. The adsorption process was studied using isotherm and kinetic models to assess the effectiveness of the adsorbent, which would result in key information for developing an adsorption system [31].

■ EXPERIMENTAL SECTION

Materials

Apple waste from the *Manalagi* apples was collected from Batu, Malang. Guardia et al. [32] examined the elemental analysis of an apple, which is composed of 47.1% carbon, 6.4% hydrogen, 0.5% nitrogen, and 46.0% oxygen. Suarez-Garcia et al. [26] did a biopolymer analysis and found that it is made up of 44.0% holocellulose, 17.3% lignin, 6.7% soluble in organic solvents, and 31.3% soluble in water. The analytical grade materials used for this study included malachite green powder (Merck) and 2% w/v NaOH (Merck). Other materials, such as 0.1 M phosphate buffer pH 7.4 (Muda Berkah group) and aquadest (WaterOne), are technical grade.

Instrumentation

A JEOL JSM-IT510LV scanning electron microscope-energy dispersive X-rays (SEM-EDS) were used in this study. A Quantachrome Novatouch Lx4 surface area analyzer was also used, as well as Fourier-transform infrared radiation (FTIR) with a Perkin Elmer Spectrum Two System L160000A. The EDAQ Potentiostat was used to measure the concentration of malachite green at equilibrium. The GCE electrode was used as the working electrode, the Ag|AgCl electrode was used as the reference electrode, and the Pt wire electrode was used as the counter electrode.

Procedure

Preparation of apple wastes

As much as 3 kg of apple waste were air-dried for 3 d and then dried at 110 °C for 48 h. We ground the dried apple wastes into fine powder using a food processor and sifted them through a mesh of 100 to achieve uniform particles.

Production of AC

Powdered apple wastes were carbonized in the furnace at 800 °C for 1 h. The carbon obtained from this step was divided into two parts. One division was kept aside for the adsorption process and labeled AC. The other part endured additional activation with NaOH 0.5 M and was labeled AC-NaOH. These adsorbents were soaked in the solution for 24 h, washed with aquadest, and dried at 110 °C for 3 h.

Characterization

All variants of the adsorbents were examined using FTIR spectroscopy, surface area analysis, and SEM-EDS. All adsorbent characterization results are compared to extract information about the adsorbent. FTIR spectroscopy was supposed to characterize the adsorbents chemically by determining their functional groups. The infrared transmission spectrum was recorded from 400 to 4000 cm^{-1} using the KBr wafer technique. The surface area analyzer (SAA) used N_2 gas adsorption-desorption at 77 K to look at the adsorbents and figure out their surface area and porous volume. Before the adsorption, samples of adsorbents were degassed under vacuum at 473.15 K for 6 h. The BET isotherm identified the adsorbents' surface area. The t-plot and the Barrett-Joyner-Halenda (BJH) model were used to find the adsorbents' average pore diameter, micropore volume, and micropore area. The SEM instrument was utilized to magnify the adsorbent 1000 and 5000 times. The EDS spectrum detected the elements and determined their percentages in these samples.

Determination of the optimum conditions with batch method

Adsorbents labeled as AC and AC-NaOH underwent adsorption processes to determine the optimum adsorption conditions. The batch method was used to help determine these conditions. The experiment was carried out by varying the mass of the adsorbent, the contact time, and the initial concentration of malachite green.

Determination of the optimum mass of the adsorbent

Adsorbent samples with masses of 0.1, 0.2, 0.3, 0.4, and 0.5 g were added to flasks filled with 50 mL of malachite green 50 ppm and shaken at 100 rpm for 30 min. After the adsorption process, the solutions were filtered and kept aside.

Determination of the optimum contact time

Adsorbent samples with the optimum mass were added to flasks filled with 50 mL of malachite green at 50 ppm, then shaken with the shaker at 100 rpm for 10, 20, 30, 40, 50, and 60 min. After the adsorption process, the solutions were filtered and kept aside

Determination of the optimum adsorbate concentration

The optimum amount of adsorbent samples was put into flasks that were 50 mL full of 50, 100, 150, 200, 250, and 300 ppm malachite green. The flasks were then shaken at 100 rpm for the optimum time. After the adsorption process, the solutions were filtered and kept aside. The concentration of the filtrates was determined with cyclic voltammetry. Standard curves for both methods were created by making standard solutions and measuring their peak current with a scan rate of 200 mV/s. At least 25.0 mL of these filtrates were used in cyclic voltammetry with 5.0 mL of 0.1 M phosphate buffer 7.4 as the electrolyte.

Adsorption isotherm and kinetics

The data obtained from determining the optimum concentration experiment were modeled into eight isotherms to identify the most suitable isotherm model to describe the adsorption. Langmuir, Freundlich, Temkin, Dubinin-Radushkevich, BET, Hill de Boer, Redlich-Peterson, and Sips are the isotherm models used. Table 1 summarizes the linear equations of all isotherm models used in this experiment and their parameters. Eq. (1) and Eq. (2) calculated the adsorption capacity and the removal capacity, respectively.

$$Q = \frac{(C_0 - C_t)}{w} \times V \quad (1)$$

$$\text{Removal efficiency}(\%) = \frac{(C_0 - C_t)}{C_0} \times 100\% \quad (2)$$

In which C_0 represents the concentration of malachite green initially (ppm), C_t denotes the concentration of malachite green at equilibrium (ppm), w stands for the adsorbent's mass (g), and V symbolizes the volume of the solution (L). The isothermal analysis of the adsorption data was carried out by fitting them into the isotherm linear equations.

The kinetics of adsorption provide insights into potential adsorption mechanisms and are crucial for determining suitable process parameters and optimal conditions for larger-scale removal processes [33]. The kinetic models derived from the adsorption data include pseudo-first-order, pseudo-second-order, and intraparticle diffusion models. Table 2 presents the linear equations corresponding to the specified kinetics models.

■ RESULTS AND DISCUSSION

FTIR Analysis

Fig. 1 shows the FTIR spectrum of AC. It has strong and wide peaks at 3400 cm^{-3}, which points to the

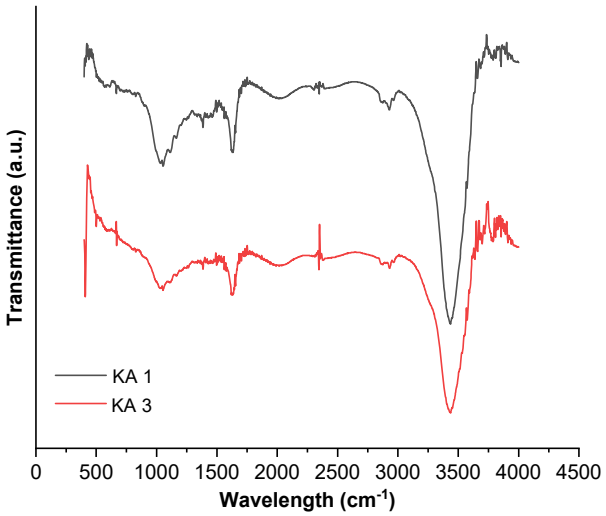

Fig 1. FTIR spectrum of AC and AC -NaOH

Table 1. Linear form of isotherm models and their parameters

Isotherm	Linear equation	Plot	Parameters
Langmuir	$\frac{C_e}{q_e} = \frac{1}{K_L q_m} + \frac{C_e}{q_m}$	C_e vs. $\frac{C_e}{q_e}$	q_m, K_L, R_L
Freundlich	$\log q_e = \log K_F + \frac{1}{n}\log C_e$	$\log C_e$ vs. $\log q_e$	K_F, n
Temkin	$q_e = B\ln A_T + B\ln C_e$	$\ln C_e$ vs. q_e	A_T, B_T
Dubinin-Radushkevich	$\ln q_e = \ln q_m + \beta\varepsilon^2$	ε^2 vs. $\ln q_e$	K_{DR}, q_s, E
Redlich-Peterson	$\ln\frac{C_e}{q_e} = \beta\ln C_e - \ln\alpha R$	$\ln C_e$ vs. $\ln\frac{C_e}{q_e}$	αR, β
Hill-de Boer	$\ln\left[\frac{C_e(1-\theta)}{\theta}\right] - \frac{\theta}{1-\theta} = \ln K_1 - \frac{K_2\theta}{RT}$	θ vs. $\ln\left[\frac{C_e(1-\theta)}{\theta}\right] - \frac{\theta}{1-\theta}$	K_1, K_2
Sips	$\ln\left(\frac{q_e}{q_m - q_e}\right) = \beta_s \ln C_e + \ln K_s$	$\ln C_e$ vs. $\ln\left(\frac{q_e}{q_{max} - q_e}\right)$	q_m, β_s, K_s

Table 2. Linear form of kinetics models and their parameters

Isotherm	Linear equation	Plot	Parameters
Pseudo-first-order	$\ln(q_e - q_t) = \ln q_e + k_1 t$	t vs. $\ln(q_e - q_t)$	q_e, k_1
Pseudo-second-order	$\frac{t}{q_t} = \frac{1}{k_2 q_e^2} + \frac{1}{q_e}t$	t vs. $\frac{t}{q_t}$	q_e, k_2
Intraparticle diffusion	$q_t = K_p\sqrt{t} + C$	$\sqrt{t}$ vs. q_t	K_p, C

O–H vibrational stretch. The peak at 2928 cm^{-1} shows an aliphatic C–H stretch. There is also a possibility of a C=C bond for the peak at 1626 cm^{-1}. The peak at 1384 cm^{-1} came from tertiary alcohol or phenol, made it more likely that the adsorbent has an O–H bond. The peak at 1053 cm^{-1} implies the C–O–C and O–H bond vibration from polysaccharides.

AC-NaOH, as shown in Fig. 1, has similar peaks to AC, which means a chemically activated adsorbent would still have the same functional groups. Some peaks in AC, such as the one at 3400 cm^{-1}, are not as broad. The same goes for the aliphatic C–H stretch. Chemical activation helped form new functional groups, the 2345 and 669 cm^{-1} peaks. The peak at 2345 cm^{-1} indicates the existence of C≡C, whereas the peak at 669 cm^{-1} indicates out-of-plane bending by alcohol.

Apple waste approximately comprised 46% oxygen, indicating the presence of hydroxyl, ether, and carbonyl groups [34]. The diminution of the –OH peak, C–O–C bonds, C=O, and aliphatic C–H groups post-activation signifies that the activation-induced the decarboxylation and dehydration of lignocellulosic constituents [35]. Weaker oxygen-containing bonds are broken down to facilitate the formation of more aromatic compounds. In this instance, NaOH was a catalyst to decompose these oxygen-containing bonds. In conjunction with thermal treatment, NaOH induces dehydration, facilitating oxygen loss and transforming carbon into more condensed structures [36]. The creation of condensed structures and the breakdown of lignocellulosic compounds result in the formation of C≡C bonds. Hafizuddin et al. [37] propose the activation method with NaOH, detailing the reactions in Eq. (3–6).

$$4NaOH + C \rightarrow Na_2CO_3 + Na_2O + 2H_2 \quad (3)$$

$$2Na_2O + C \rightarrow 4Na + CO_2 \quad (4)$$

$$Na_2CO_3 + 2C \rightarrow 2Na + 3CO \quad (5)$$

$$C + CO_2 \leftrightarrows 2CO \quad (6)$$

These reactions result in the degradation of the less stable organic molecules, facilitated by NaOH as the activating agent. Consequently, the NaOH activation did not compromise the entire carbon structure due to its selectivity and promoted the formation of a porous structure [21]. The development of a condensed structure contributed to structural integrity; hence, it maintained the integrity of AC.

SEM-EDS

According to the morphologies displayed in Fig. 2, AC-NaOH has enlarged and deeper pores than AC. These pores significantly affect the adsorption of malachite green, giving the adsorbate additional space to stick to the adsorbent's surface. Based on the EDS spectra shown in Fig. 3, both adsorbents contain a high amount of carbon: 88.67% (AC) and 94.42% (AC-NaOH). The adsorbents fulfilled the SNI 06-3730-1995 criteria, which stated that good AC should contain at least 65% of the total carbon. The EDS spectrum also identified some minerals (Mg, K, and Ca) contained in ordinary AC, which were later removed due to chemical activation.

A notable distinction between AC and AC-NaOH lies in the composition of carbon and oxygen in the two adsorbents. AC contained the least amount of carbon but the highest number of oxygen. AC-NaOH had the highest percentage of carbon, which could be inferred as the adsorbent with the best performance [38]. The fact that both ACs had a low percentage of oxygen proved that

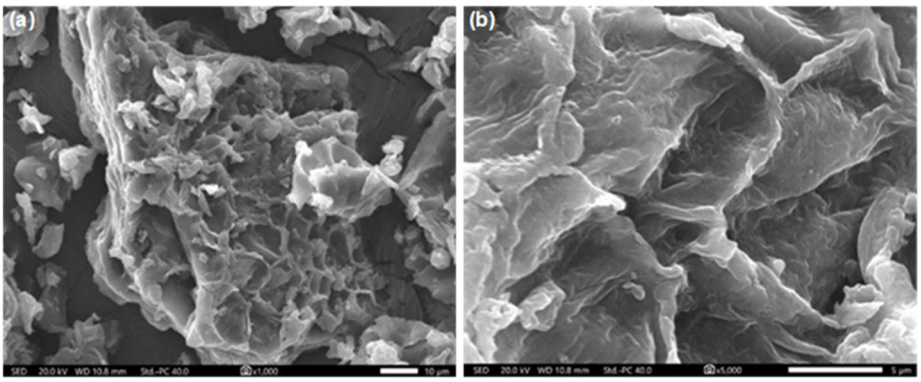

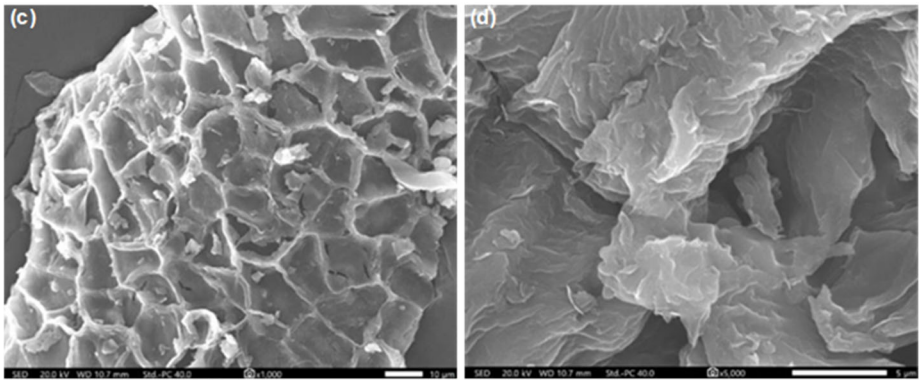

Fig 2. Morphology of (a) AC 1000×, (b) AC 5000×, (c) AC-NaOH 1000×, and (d) AC-NaOH 5000×

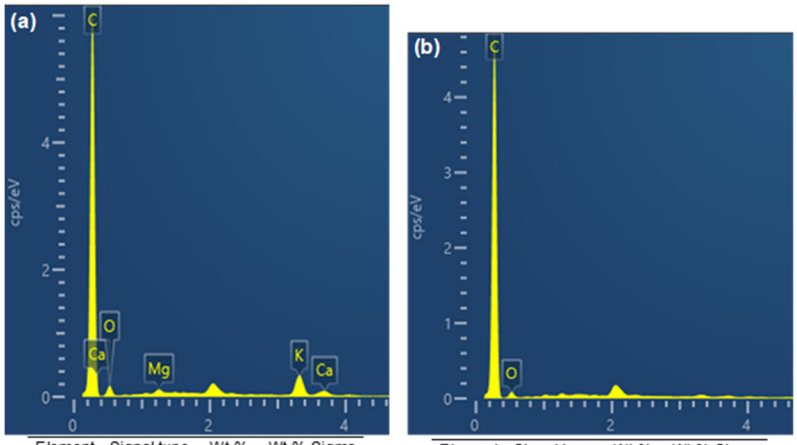

Element	Signal type	Wt.%	Wt.% Sigma
C	EDS	88.67	0.83
O	EDS	8.13	0.83
Mg	EDS	0.28	0.07
K	EDS	2.34	0.13
Ca	EDS	0.58	0.09
Total		100.00	

Element	Signal type	Wt.%	Wt.% Sigma
C	EDS	94.42	0.77
O	EDS	5.58	0.77
Total		100.00	

Fig 3. EDS spectrum analysis of (a) AC and (b) AC-NaOH

the lignin and cellulose compounds were dehydrated, which was also supported by the FTIR results.

SAA Analysis

Characterization of the two adsorbents with a SAA provides information about the adsorbent's surface area, pore distribution, BET isotherm, and type of isotherm. The N_2 adsorption-desorption graphs are illustrated in Fig. 4. The N_2 adsorptions, which began at $p = 0.05$ atm until 1 atm, show sharp inclines of adsorbed volumes, which gradually declined as the pressure increased. However, there are also increases in high pressures. The desorption rate did not match the adsorption rate, potentially due to insufficient degassing time. Another factor that caused these conditions is that the pore's diameter is larger than the pore's neck, which would indicate that the pores are ink-bottle shaped, typically occurring in ACs [39]. Ink-bottle-shaped pores were usually mesopores, indicating that these adsorbents followed the type IV isotherm, according to IUPAC [40]. Table 3 displays the textural parameters of both adsorbents using the N_2 adsorption-desorption isotherm, t-plot, BET, and BJH analyses.

According to the textural parameters, chemical activation increased the adsorbent's surface area. The volume of the pores also appears to be deeper compared to AC, which validates the SEM-EDS analysis. The radius of the pores, which are more than 2 nm, supports the assumption that both adsorbents are mostly mesopores. According to the IUPAC classification [40], adsorbents with pore diameters larger than 2 nm and smaller than 50 nm are classified as mesopores.

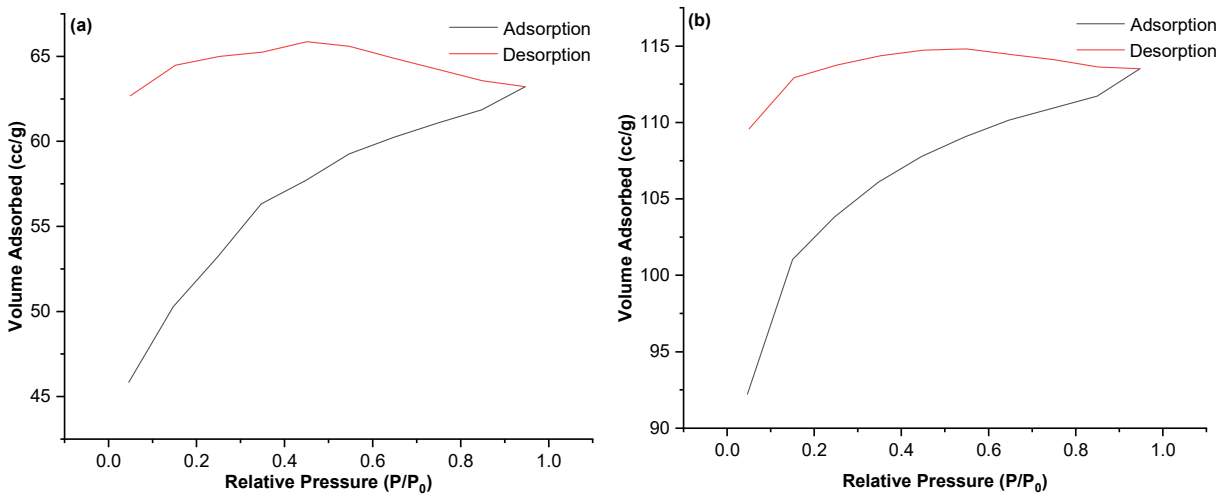

Fig 4. N_2 adsorption-desorption isotherm graph of (a) AC and (b) AC-NaOH

Table 3. Textural parameters of AC and AC-NaOH

Sample	AC	AC-NaOH
S_{BET} (m^2/g)	159.232	299.203
V_{total} (cc/g)	0.0980367	0.176021
APR_{BJH} (nm)	2.03422	2.02913

Even though the surface area and the total volume increased due to chemical activation, the radius of AC-NaOH is smaller than AC. The increase in depth caused the increase in the surface area, which is supported by the total volume data. In conclusion, the SAA results indicated that AC-NaOH exhibited superior characteristics compared to AC, which was consistent with the experimental findings. This result also means that chemical activation with a base could improve the performance of AC in adsorbing textile dyes, such as malachite green. Table 4 displays the BET parameters of other AC recently in comparison to AC-NaOH.

AC-NaOH surpasses the characteristics of ACs sourced from several sources, including tea waste and almond shells. While research conducted by Venkatesan et al. [24] and Tran et al. [43] yielded ACs with better surface areas, the AC-NaOH produced from apple waste in this study remains comparable to viable adsorbents, as the difference in surface areas and pore volumes may be attributed to differences in the activation methods used.

Malachite Green Calibration Curve from Cyclic Voltammetry

This experiment's voltammetry conditions were based on similar research [44], which identified the best peaks under those conditions. The cyclic voltammograms obtained from malachite green standard solutions are portrayed in Fig. 5. The changes between the concentrations of the malachite green cyclic voltammograms were slight since this experiment used relatively small concentrations as standards. Based on the cyclic voltammograms, a standard curve can be made by extracting the peaks from the voltammograms. The peaks obtained from the voltammograms are summarized in Table 5, and the standard curve is shown in Fig. 6. The cyclic voltammograms of malachite green at conditions stated in the experimental section showed

Table 4. BET comparison of AC and their activation method

Material	Activation method	S_{BET} (m^2/g)	V_{total} (cc/g)	Reference
Apple waste	0.5 M NaOH (24 h)	299.2030	0.1760	This work
Tea waste	NaOH ratio 1:1 (24 h)	270.0000	0.1060	[41]
Almond shell	400 °C (75 min)	120.2100	0.5720	[42]
Cotton stalk	H_3PO_4 ratio 1:2 (24 h)	461.0000	1.2190	[24]
Dragon fruit peel	NaOH 24 h at 100 °C, 600 W (2 min)	688.8080	0.0158	[43]

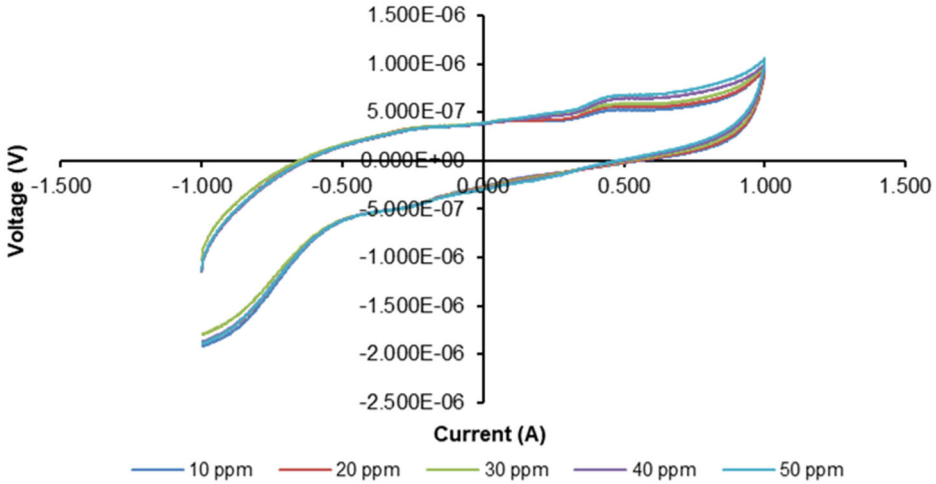

Fig 5. Cyclic voltammograms from malachite green standard solutions

Table 5. Peaks from malachite green cyclic voltammograms

No	Standard conc. (ppm)	Peak (μA)
1	10	0.52150623322
2	20	0.56100624085
3	30	0.58045623779
4	40	0.63722187042
5	50	0.66879371643

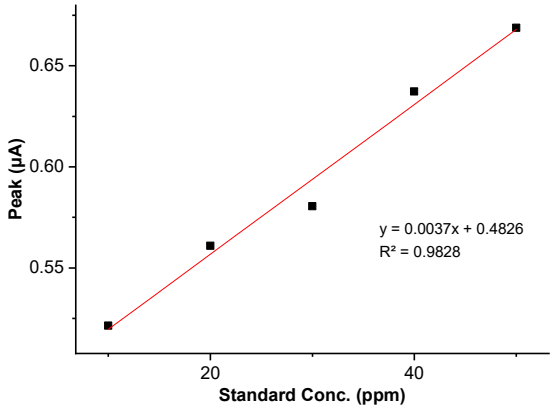

Fig 6. Calibration curve of malachite green from standard solutions

an anodic peak. This anodic peak is due to the oxidation of the carbinol form of malachite green [44]. Based on the lack of cathodic peaks, the reaction during the cyclic voltammogram readings is irreversible [45].

The calibration curve was plotted against the standard concentration, ranging from 10 to 50 ppm. With a correlation coefficient of 0.9828, the plot demonstrated exceptional linearity. This result means that cyclic voltammetry is a valid method for measuring the unknown malachite green concentration after the adsorption process.

Batch Method Optimum Conditions

Influence of adsorbent mass on adsorption

The results of determining the optimum adsorbent mass experiment are summarized in Fig. 7. The findings show that 0.3 g of adsorbent are needed to adsorb 50 mL of malachite green solution at 50 ppm for 30 min with the removal efficiency of 95.312% (AC) and 95.577% (AC-NaOH). At those particular masses, the adsorption capacities are 8.009 mg/g (AC) and 8.016 mg/g (AC-NaOH).

Typically, adding more adsorbent could increase the surface area, thus increasing existing adsorption sites [46]. The malachite green adsorption followed that notion until the optimum adsorbent dose; then, the adsorption efficiency dropped afterward. There are more unsaturated adsorption sites [47-48], which means that more adsorbents could be used and allow particles to build up. This is what causes the lower efficiency. The concentration of the adsorbate did not rise linearly with the surface area. After absorbing most of the adsorbate, the remaining particles moved slower [49]. Thus, the adsorption capacity will decrease, as reflected in the results of this experiment.

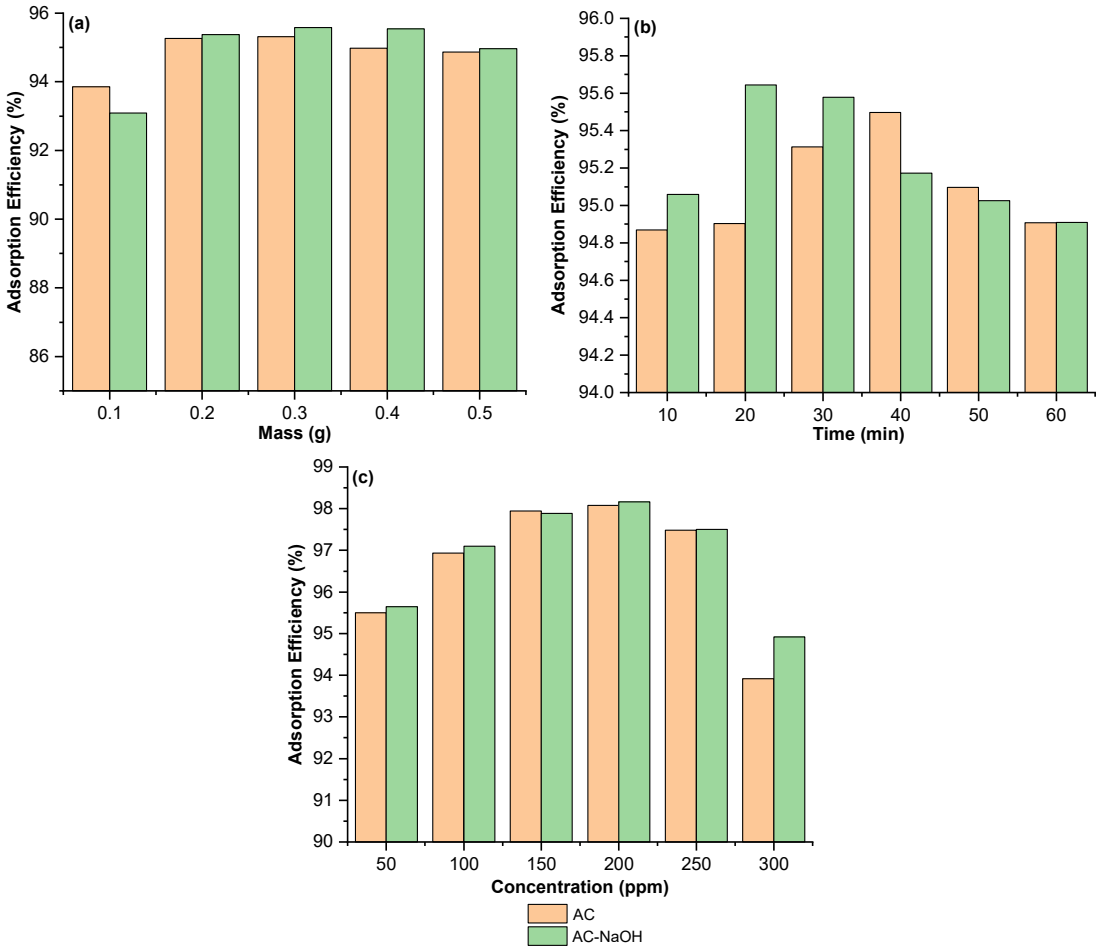

Fig 7. The influence of (a) adsorbent mass, (b) contact time, and (c) adsorbate dose on the adsorption efficiency

Influence of contact time on adsorption

According to these cyclic voltammetry results, the optimum contact time to adsorb the same amount and volume of malachite green is 0.3 g, with a removal efficiency of 95.312% (AC) and 95.577% (AC-NaOH). At that particular mass, the adsorption capacities are 8.009 mg/g (AC) and 8.016 mg/g (AC-NaOH).

Based on the results, the adsorption capacity dropped after reaching the optimal contact time. Occasionally, the adsorption process can go on longer than the ideal contact time. This condition can cause the adsorbate-adsorbent complex to break up into adsorbent and adsorbate molecules during the desorption process [50]. Furthermore, the adsorption active sites could be full, which means they cannot hold any more adsorbate molecules [51].

Influence of adsorbate dose on adsorption

According to these cyclic voltammetry results, the optimum adsorbent dose with the optimum adsorbent dose and contact time for each adsorbent is 200 ppm with a removal efficiency of 98.081% (AC) and removal efficiency of 98.165% (AC-NaOH). At that concentration, the adsorption capacities are 32.905 mg/g (AC) and 32.933 mg/g (AC-NaOH).

The adsorption capacity for both adsorbents sharply declined after reaching the optimum adsorbate dose. This phenomenon is due to insufficient active sites, as the adsorption sites were fully saturated. If the adsorbate dose was raised above the optimal amount and there were not enough adsorption sites, the adsorption efficiency would decrease because the active sites could not handle more adsorbate molecules [52].

It was shown in all three experiments that AC mixed with 0.5 M NaOH is the best adsorbent because it works better, takes less time, and requires less effort. There is evidence that adding NaOH to the activation process effectively removes unwanted substances from the AC and makes its pores bigger. NaOH acted as a dehydrating agent during the activation process, breaking the C–C and C–O–C bonds in the carbon and promoting more extensive pore formation [30].

Evaluation of the Adsorption Isotherm and Kinetics

The experiment results to find the best adsorbate dose are plotted against the adsorption isotherm models to see which best describes the adsorption process. The graphs from the isotherm models can be seen in Fig. 8, and the parameters for both adsorbents were found in Table 6 and based on the linear graphs.

Out of those seven isotherms listed, no isotherm models could fulfill the correlation coefficient requirement for the adsorption that happened with AC. Hill de Boer is the closest isotherm model to linearity for this adsorption, with $R^2 = 0.8724$. Based on the positive K_2 parameter, it appears that there are attractive forces between adsorbate species [53]. The Temkin isotherm is another isotherm that showed fairly excellent linearity with the adsorption data, with $R^2 = 0.7891$. This isotherm provides information about the relationship between the heat of adsorption and surface coverage; in this case, the heat of adsorption will decrease linearly [54]. Based on the parameter BT, the adsorption type was physisorption since BT < 8 kJ/mol [55]. Although this notion contradicts the parameter results from the Dubinin-Radushkevich isotherm, the Temkin isotherm fits the adsorption data better. The adsorption data fit decently with the Sips isotherm. The parameter is less than 1, indicating lateral interactions between adsorbate molecules and the adsorbent. The result also provides insight into adsorption occurring at a homogenous surface [56].

Table 6. Isotherm parameters for the adsorption of malachite green

Isotherm	Parameter	AC	AC-NaOH
Langmuir	q_m (mg/g)	78.125000	95.238100
	K_L (L/mg)	0.0979342	0.07703595
	R_L	0.0194850	0.0194850
	R^2	0.5515000	0.3845000
Freundlich	K_F (mg/g)	8.4469510	7.7535390
	n	1.4507470	1.2963440
	$\frac{1}{n}$	0.6893000	0.7714000
	R^2	0.6191000	0.6668000
Temkin	A_T (L/mg)	1.0939930	0.9764460
	B_T (J/mol)	141.80890	127.17110
	R^2	0.7891000	0.8337000
Dubinin–Radushkevich	K_{DR} (mol²/kJ²)	0.000000005	0.00000001
	q_m (mol/g)	0.0040410	0.0030720
	E (J/mol)	10000.000	6930.0000
	R^2	0.6414000	0.9996000
Redlich–Peterson	αR	8.446904138	7.788902779
	β	0.3107000	0.2332000
	R^2	0.2481000	0.1533000
Hill-de Boer	K_1	1227.948292	3588.896
	K_2	31051.36082	37509.96535
	R^2	0.8724000	0.8144000
Sips	q_m (mg/g)	35.96839005	59.54648249
	β_s	1.07342207	0.927127758
	K_s	0.133694224	0.075215346
	R^2	0.7766000	0.7357000

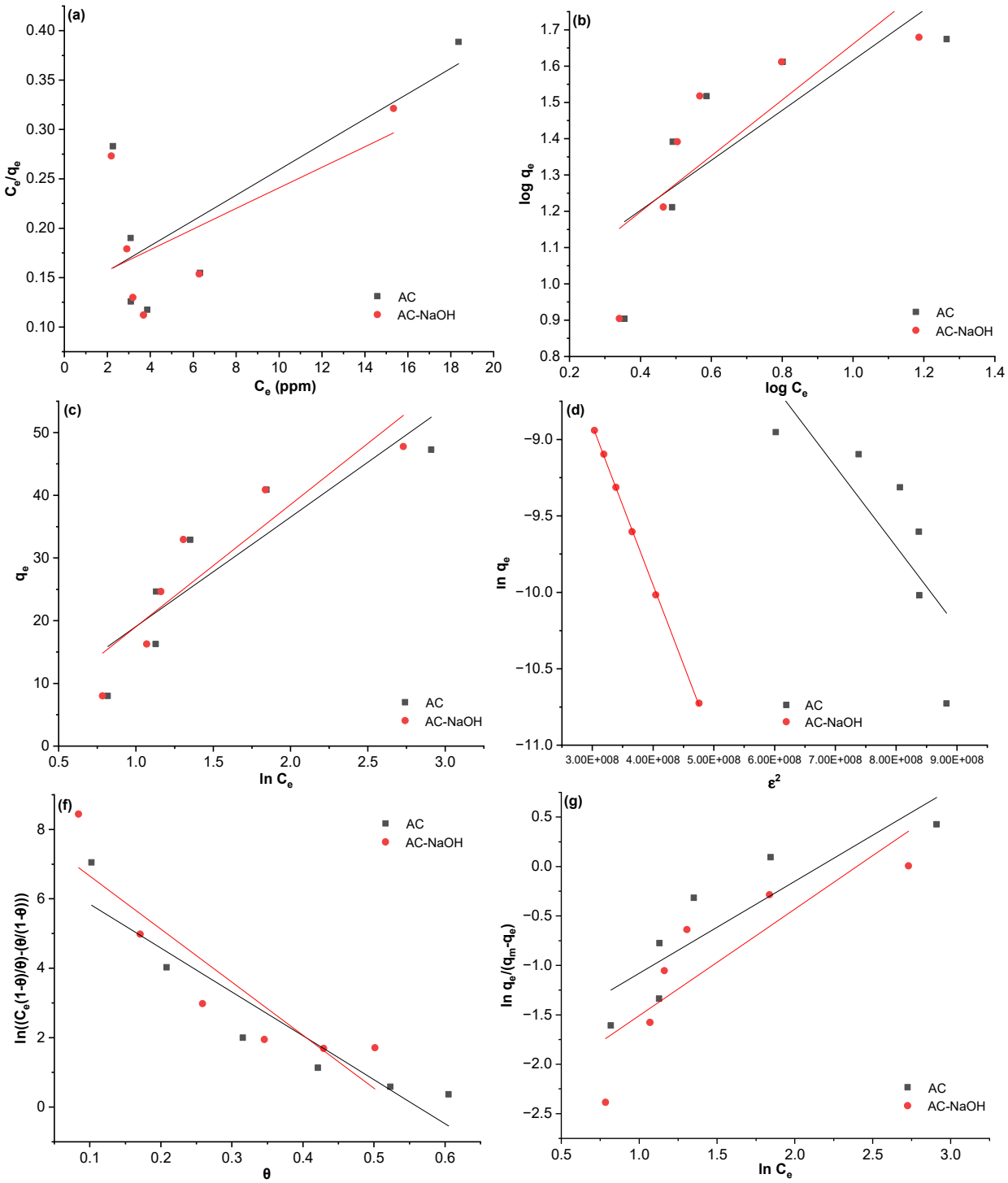

Fig 8. Linear graphs of (a) Langmuir, (b) Freundlich, (c) Temkin, (d) Dubinin-Radushkevich, (e) Redlich-Peterson, (f) Hill-de Boer, and (g) Sips models

The isotherm model that best fits the adsorption with AC-NaOH is the Dubinin-Radushkevich isotherm. According to the E parameter in the Dubinin-Radushkevich, which was < 8 kJ, the type of adsorption that happened was physisorption [57]. This notion is also supported by the results of the Temkin isotherm, which also showed fairly decent linearity. The Freundlich isotherm values, which are more linear than

the Langmuir isotherm values, show that adsorption with AC-NaOH is more likely to form a multilayer than a monolayer.

On other similar studies [10,58], the q_m is deduced from the Langmuir isotherm. Multilayers and surface heterogeneity are present in the adsorption; hence, the Langmuir isotherm has poor linearity. As a consequence, there is a notable difference in q_m values between the batch method and the Langmuir isotherm. This discrepancy is caused by the linear analysis of the data, which can introduce errors [59]. Although linear regression of the adsorption models is easier and more convenient, this linearization changes the dependent and independent variables of the adsorption [60]. Table 7 displays a comparison of the adsorbents used for malachite green adsorption. AC-NaOH significantly outperforms the other adsorbents in terms of malachite green adsorption capability. The AC generated in this study is a highly efficient and effective adsorbent that utilizes apple trash, hence rendering it cost-effective.

Fig. 9 displays the BET isotherm for two adsorbents obtained from the SAA, which produced excellent results. The correlation coefficients of the two adsorptions are $R^2 = 0.997291$ (AC) and $R^2 = 0.994673$ (AC-NaOH). The BET isotherm is typically used to describe physisorptions [64]. The BET isotherms show that physisorption is present in the adsorption on a homogenous surface, and there is a tendency to build multilayers. On the other hand, the Dubinin-Radushkevich isotherm for AC-NaOH is very linear, suggesting that micropores drive the adsorption [65], which opposes the BET isotherm. This is because the isotherm was designed for solids with micropores. Since both isotherms showed excellent linearity, even if the micropore-filling mechanism is dominant, mesopores are still responsible for the adsorption process. Hence, multilayers are formed on top of the mesopores and external surfaces.

Adsorption with AC, however, suggests that mesopores and macropores are more inclined to influence the adsorption process, which would allow

Table 7. q_m Comparison of the adsorbents in malachite green adsorption

Material	Activation conditions	Isothermal model	q_m (mg/g)	Reference
Apple waste	0.5 M NaOH (24 h)	Dubinin-Radushkevich	95.24	This work
Mangosteen peel	1% $NaHCO_3$ (24 h)	Temkin	19.35	[61]
Charcoal	200 °C (15 h)	Dubinin-Radushkevich	62.19	[58]
Sugarcane bagasse	0.5 g SnO_2 (1 h)	Langmuir	73.86	[10]
Kaolin clay	0.1 M HCl (48 h)	Freundlich	18.52	[62]
Lightweight expanded clay aggregate (LECA)	3.5 M KOH (2 h)	Langmuir	43.10	[63]

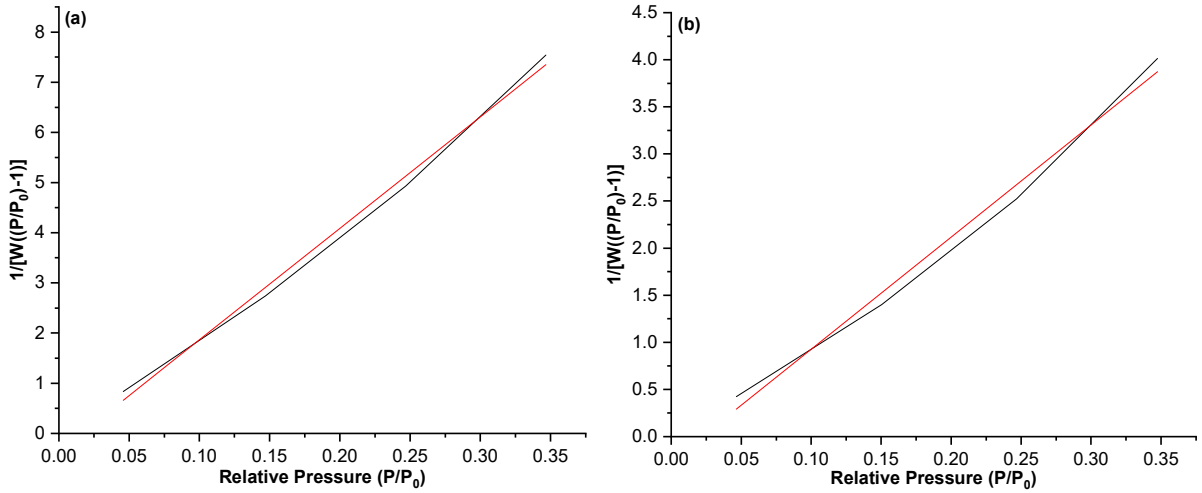

Fig 9. BET isotherm linear graphs of (a) AC and (b) AC-NaOH

multilayers to form. The micropore adsorption is not as prevalent as AC-NaOH, due to the poor Dubinin-Radushkevich isotherm fit. Judging from the adsorption energy, it appears that there are some chemisorption interactions since E > 8 kJ/mol [55]. The information obtained from the BET isotherm supported the conclusion from the Sips isotherm that a homogenous surface is present on AC.

The parameters of the adsorption kinetics were derived from the data obtained during the optimal contact time experiment, utilizing the linear equations shown in Table 2. Fig. 10 illustrates the adsorption kinetics linear graphs, while Table 8 presents the corresponding parameters.

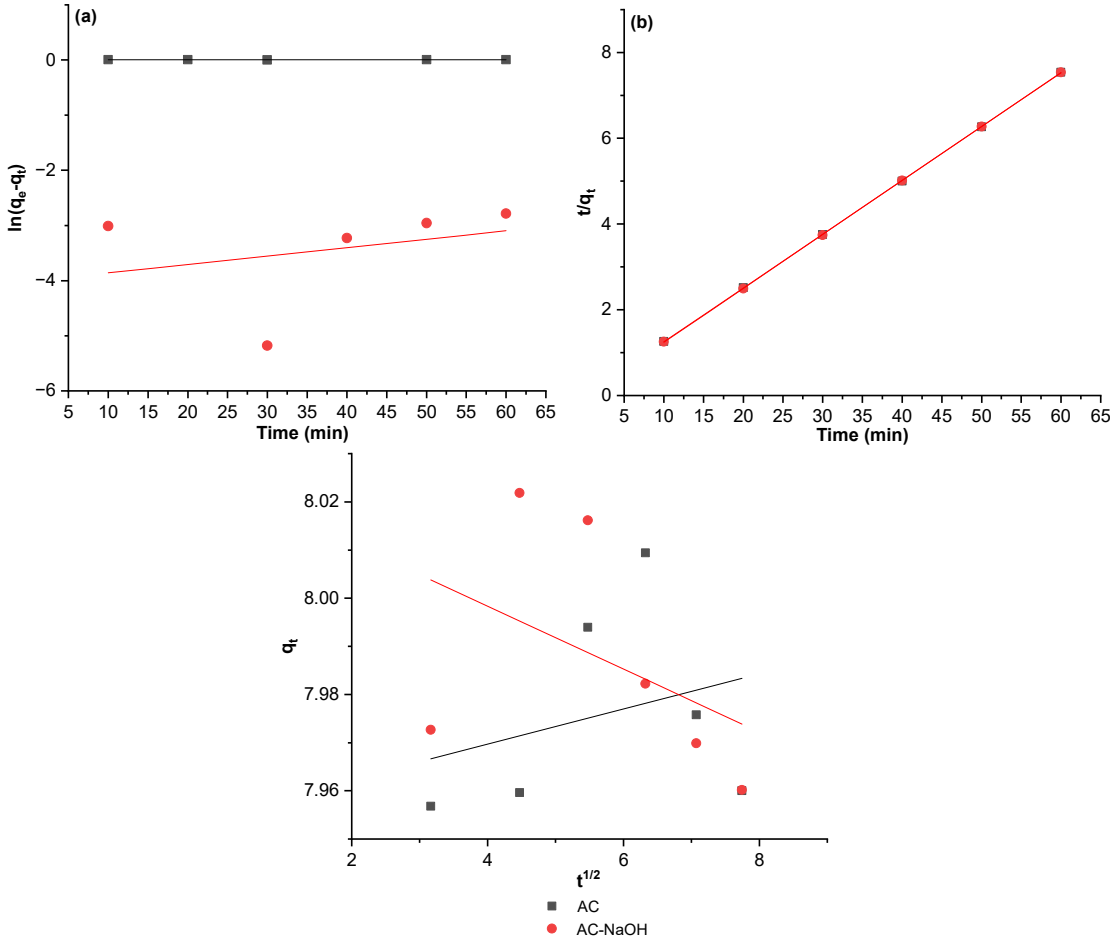

Fig 10. Linear graphs of (a) pseudo-first-order, (b) pseudo-second-order, and (c) intraparticle diffusion

Table 8. Kinetics parameters for the adsorption of malachite green

Kinetics	Parameter	AC	AC-NaOH
Pseudo-first-order	q_e (mg/g)	1.005214	0.018086
	K_1	0.00003	0.0152
	R^2	0.3458	0.0879
Pseudo-second-order	q_e (mg/g)	7.968127	7.949126
	K_2	3.6628	0.914777
	R^2	1.0000	1.0000
Intraparticle diffusion	K	0.0037	0.0065
	C	7.9551	8.0244
	R^2	0.0827	0.1862

All adsorption processes involving AC and AC-NaOH exhibited identical adsorption kinetics, characterized by a perfect correlation coefficient consistent with pseudo-second-order kinetics. Pseudo-second-order kinetics describes adsorption processes that require additional time to occupy the active sites on the adsorbent [66]. The correlation between the results and the adsorption kinetics suggests that the rate-limiting stage of adsorption is the ion exchange between the adsorbent and the adsorbate. This conclusion implies that both ACs exhibit chemisorption in their adsorption processes.

There is a strong link between the adsorption with AC-NaOH and the Dubinin-Radushkevich and BET isotherms. However, the kinetic model strongly suggests strong interactions between the adsorbent and the adsorbate, which means that the adsorption is site-specific rather than just pore-filling [67]. The adsorption type was a hybrid of physisorption and chemisorption, with chemisorption dominating the process. The similar assumption could also be made about the adsorption process with AC, in which the presence of interaction between adsorbate and adsorbent is validated with the compatibility with the Hill de-Boer isotherm.

The information obtained from both the isotherm and kinetic models helps explain the slight difference between the removal efficiency of AC and AC-NaOH despite a substantial difference in their surface area. Since the adsorption is dominated by chemisorption, the surface chemistry matters more than the surface area. There are also tendencies to build multilayers for both adsorbents, supported by the Hill de Boer (AC) and the Dubinin-Radushkevich isotherm (AC-NaOH). Hence, the need for a high surface area is not prevalent.

Proposed Adsorption Mechanism

The proposed mechanism for the adsorption of malachite green using AC-NaOH is depicted in Fig. 11, based on data from the adsorption isotherms, kinetics, and characterization studies, particularly FTIR. The process involves both chemisorption and physisorption. The chemisorption process entailed π-π interactions between

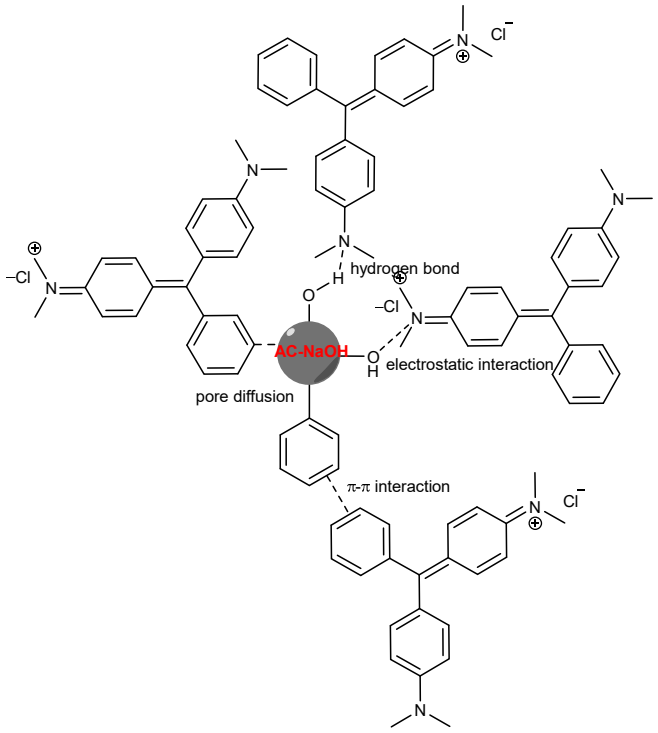

Fig 11. Proposed mechanism for malachite green adsorption with AC-NaOH

the C=C bond of AC-NaOH and the dye, hydrogen bonding between the hydroxyl group and the dimethylamino group in the malachite green structure, and electrostatic interactions between the negatively charged AC and the cationic dye malachite green [68]. Conversely, the physisorption process entails a pore diffusion validated by the Dubinin-Radushkevich isotherm. Additional weak electrostatic interactions, including dipole-dipole interactions, van der Waals forces, and London dispersion forces, are also present [69].

Other studies concerning the adsorption of malachite green using AC indicated an identical mechanism [68-70]. Certain research concurred that pore filling mechanisms and weak electrostatic interactions are present in the adsorption process, suggesting that ACs are effective for wastewater treatment [68-69]. The AC-NaOH generated from apple waste exhibits significant potential in wastewater management, particularly for the removal of malachite green dye, by demonstrating processes akin to those in known studies based on the overall experimental results.

■ CONCLUSION

This experiment demonstrated the efficient production of AC from apple wastes through carbonization and chemical activation. AC-NaOH showed the best results with the optimum conditions of 0.3 g, 40 min, and 200 ppm. The best isotherm to describe the adsorption with AC-NaOH is the Dubinin-Radushkevich and BET isotherm. The adsorption followed the pseudo-second-order kinetics, which means that the adsorption that took place was a hybrid of physisorption and chemisorption. Chemical activation with NaOH was proven to help create deeper pores and a larger surface area. The types of pores in the AC were mostly mesopores, and adsorption followed the type IV IUPAC isotherm.

■ ACKNOWLEDGMENTS

The authors are thankful to Yogyakarta State University, Indonesian Islamic University, and "Veteran" University of National Development Yogyakarta for providing the laboratory facilities and instruments as part of this research.

■ CONFLICT OF INTEREST

The authors declare that there no conflict of interest.

■ AUTHOR CONTRIBUTIONS

Narayani Balasubramaniam conducted the experiment, made calculations, and wrote the manuscript. Isana Supiah Yosephine Louise revised the manuscript and conducted final assessments of the data.

■ REFERENCES

[1] Basuki, T.M., Indrawati, D.R., Nugroho, H.Y.S.H., Pramono, I.B., Setiawan, O., Nugroho, N.P., Nada, F.M.H., Nandini, R., Savitri, E., Adi, R.N., Purwanto, P., and Sartohadi, J., 2024, Water pollution of some major rivers in Indonesia: The status, institution, regulation, and recommendation for its mitigation, *Pol. J. Environ. Stud.*, 33 (4), 3515–3530.

[2] Kumar, R., Tripathi, Y.C., Ambika, A., Sharma, J., Kumari, B., and Pandey, A., 2017, Isolation of dye from sporophore of *Xylaria polymorpha* for textile dyeing and spectrophotometric characterization of dyed fabrics, *J. Adv. Microbiol.*, 3 (4), 162–173.

[3] Chieng, H.I., Lim, L.B.L., and Priyantha, N., 2015, Enhancing adsorption capacity of toxic malachite green dye through chemically modified breadnut peel: Equilibrium, thermodynamics, kinetics and regeneration studies, *Environ. Technol.*, 36 (1), 86–97.

[4] Oyelude, E.O., Awudza, J.A.M., and Twumasi, S.K., 2018, Removal of malachite green from aqueous solution using pulverized teak leaf litter: Equilibrium, kinetic and thermodynamic studies, *Chem. Cent. J.*, 12 (1), 81.

[5] Gharavi-nakhjavani, M.S., Niazi, A., Hosseini, H., Aminzare, M., Dizaji, R., Tajdar-oranj, B., and Mirza Alizadeh, A., 2023, Malachite green and leucomalachite green in fish: A global systematic review and meta-analysis, *Environ. Sci. Pollut. Res.*, 30 (17), 48911–48927.

[6] Zhang, H., Zhang, F., and Huang, Q, 2017, Highly effective removal of malachite green from aqueous solution by hydrochar derived from phycocyanin-extracted algal bloom residues through hydrothermal carbonization, *RSC Adv.*, 7 (10), 5790–5799.

[7] Al-Tohamy, R., Ali, S.S., Li, F., Okasha, K.M., Mahmoud, Y.A.G., Elsamahy, T., Jiao, H., Fu, Y., and Sun, J., 2022, A critical review on the treatment of dye-containing wastewater: Ecotoxicological and health concerns of textile dyes and possible remediation approaches for environmental safety, *Ecotoxicol. Environ. Saf.*, 231, 113160.

[8] Reck, I.M., Baptista, A.T.A., Paixão, R.M., Bergamasco, R., Vieira, M.F., and Vieira, A.M.S., 2020, Application of magnetic coagulant based on fractionated protein of *Moringa oleifera* Lam. seeds for aqueous solutions treatment containing synthetic dyes, *Environ. Sci. Pollut. Res.*, 27 (11), 12192–12201.

[9] Bener, S., Bulca, Ö., Palas, B., Tekin, G., Atalay, S., and Ersöz, G., 2019, Electrocoagulation process for the treatment of real textile wastewater: Effect of operative conditions on the organic carbon removal

and kinetic study, *Process Saf. Environ. Prot.*, 129, 47–54.

[10] Sharma, P., Sharma, S., Sharma, S.K., Yifei, S., Guo, F., Ichikawa, T., Jain, A., and Shrivastava, K., 2024, Evaluation of optimized conditions for the adsorption of malachite green by SnO_2-modified sugarcane bagasse biochar nanocomposites, *RSC Adv.*, 14 (40), 29201–29214.

[11] Vialkova, E., Obukhova, M., and Belova, L., 2021, Microwave irradiation in technologies of wastewater and wastewater sludge treatment: A review, *Water*, 13 (13), 1784.

[12] Sharma, M., Sondhi, H., Krishna, R., Srivastava, S.K., Rajput, P., Nigam, S., and Joshi, M., 2020, Assessment of GO/ZnO nanocomposite for solar-assisted photocatalytic degradation of industrial dye and textile effluent, *Environ. Sci. Pollut. Res.*, 27 (25), 32076–32087.

[13] Rizvi, O.S., Ikhlaq, A., Ashar, U.U., Qazi, U.Y., Akram, A., Kalim, I., Alazmi, A., Ibn Shamsah, S.M., Alawi Al-Sodani, K.A., Javaid, R., and Qi, F., 2022, Application of poly aluminum chloride and alum as catalyst in catalytic ozonation process after coagulation for the treatment of textile wastewater, *J. Environ. Manage.*, 323, 115977.

[14] Sonawane, A.V., and Murthy, Z.V.P., 2023, A metal organic framework decorated 2-dimensional nanomaterial based nanocomposite photocatalyst for photocatalytic degradation of dyes from textile industry wastewater, *Environ. Sci.: Water Res. Technol.*, 9 (10), 2515–2537.

[15] Haddaji, D., Ghrabi-Gammar, Z., Ben Hamed, K., and Bousselmi, L., 2019, A re-circulating horizontal flow constructed wetland for the treatment of synthetic azo dye at high concentrations, *Environ. Sci. Pollut. Res.*, 26 (13), 13489–13501.

[16] Kallawar, G.A., and Bhanvase, B.A., 2024, A review on existing and emerging approaches for textile wastewater treatments: Challenges and future perspectives, *Environ. Sci. Pollut. Res.,* 31 (2), 1748–1789.

[17] Yakout, S.M., and Sharaf El-Deen, G., 2016, Characterization of activated carbon prepared by phosphoric acid activation of olive stones, *Arabian J. Chem.*, 9, S1155–S1162.

[18] Bolan, N., Hoang, S.A., Beiyuan, J., Gupta, S., Hou, D., Karakoti, A., Joseph, S., Jung, S., Kim, K.H., Kirkham, M.B., Kua, H.W., Kumar, M., Kwon, E.E., Ok, Y.S., Perera, V., Rinklebe, J., Shaheen, S.M., Sarkar, B., Sarmah, A.K., Singh, B.P., Singh, G., Tsang, D.C.W., Vikrant, K., Vithanage, M., Vinu, A., Wang, H., Wijesekara, H., Yan, Y., Younis, S.A., and Van Zwieten, L., 2022, Multifunctional applications of biochar beyond carbon storage, *Int. Mater. Rev.*, 67 (2), 150–200.

[19] Hussin, F., Aroua, M.K., and Szlachta, M., 2022, Biochar derived from fruit by-products using pyrolysis process for the elimination of Pb(II) ion: An updated review, *Chemosphere*, 287, 132250.

[20] Negm, N.A., Altalhi, A.A., Ahmed, H.M., and Mohamed, E.A, 2024, Synergistic effect of rice husk-derived activated carbon modified by Ni/Al-layered double hydroxides for lead removal from industrial wastewater, *Sci. Rep.*, 14 (1), 28411.

[21] Siemak, J., Mikołajczak, G., Pol-Szyszko, M., and Michalkiewicz, B., 2024, Activated carbon for CO_2 adsorption from avocado seeds activated with NaOH: The significance of the production method, *Materials*, 17 (16), 4157.

[22] Aladeokin, O., and Fletcher, A., 2024, A novel activated carbon material from peanut shells for the removal of methyl orange and methylene blue dyes from wastewater: Kinetics, isotherms and mechanism, *Adsorpt. Sci. Technol.*, 42, 02636174241256843.

[23] Sadeghy, S., Pormazar, S.M., Ghaneian, M.T., Ehrampoush, M.H., and Dalvand, A., 2024, Modeling and optimization of direct dyes removal from aqueous solutions using activated carbon produced from sesame shell waste, *Sci. Rep.*, 14 (1), 24867.

[24] Venkatesan, A., Srividhya, B., Alajmi, A., Sadeq, A.M., Chava, R.K., Habila, M.A., Senthil Kumar, D., Guganathan, L., and Ragupathy, S., 2025, High adsorption capacities of rhodamine B dye by activated carbon synthesized from cotton stalks

agricultural waste by chemical activation, *Ceram. Int*., 51 (10), 13345–13354.

[25] Food and Agriculture Organization of the United Nations, 2024, *Fruit consumption per capita, 1961 to 2022*, https://ourworldindata.org/grapher/fruit-consumption-per-capita, accessed on January 28, 2025.

[26] Suárez-García, F., Martínez-Alonso, A., and Tascón, J.M.D., 2002, Pyrolysis of apple pulp: Effect of operation conditions and chemical additives, *J. Anal. Appl. Pyrolysis*, 62 (1), 93–109.

[27] Ramdane, N., Bouchelta, C., Marsa, Z., Medjram, M.S., and Magri, P., 2016, Production of activated carbon from apple waste prepared under N_2/microwave radiations, *J. Chem. Pharm. Res*., 8 (1), 617–627.

[28] Togibasa, O., Mumfaijah, M., Allo, Y.K., Dahlan, K., and Ansanay, Y.O., 2021, The effect of chemical activating agent on the properties of activated carbon from sago waste, *Appl. Sci.*, 11 (24), 11640.

[29] Borisut, P., Tangsathitkulchai, C., and Nuchitprasittichai, A., 2024, Dynamic of CO_2 adsorption in a fixed bed of microporous and mesoporous activated carbon impregnated with sodium hydroxide and the application of response surface methodology (RSM) for determining optimal adsorption conditions, *Environ. Sci. Pollut. Res.*, 31 (9), 13833–13855.

[30] Islam, M.A., Ahmed, M.J., Khanday, W.A., Asif, M., and Hameed, B., 2017, Mesoporous activated carbon prepared from NaOH activation of rattan (*Lacosperma secundiflorum*) hydrochar for methylene blue removal, *Ecotoxicol. Environ. Saf.*, 138, 279–285.

[31] Wang, J., and Guo, X., 2023, Adsorption kinetics and isotherm models of heavy metals by various adsorbents: An overview, *Crit. Rev. Environ. Sci. Technol.*, 53 (21), 1837–1865.

[32] Guardia, L., Suárez, L., Querejeta, N., Rodríguez Madrera, R., Suárez, B., and Centeno, T.A., 2019, Apple waste: A sustainable source of carbon materials and valuable compounds, *ACS Sustainable Chem. Eng.*, 7 (20), 17335–17343.

[33] Aslam, M.M.A., Kuo, H.W., Den, W., Sultan, M., Rasool, K., and Bilal, M., 2022, Chapter 10 - Recent trends of carbon nanotubes and chitosan composites for hexavalent chromium removal from aqueous samples, *Sep. Sci. Technol.*, 15, 177–207.

[34] Gowman, A.C., Picard, M.C., Rodriguez-Uribe, A., Misra, M., Khalil, H., Thimmanagari, M., and Mohanty, A.K., 2019, Physicochemical analysis of apple and grape pomaces, *BioResources*, 14 (2), 3210–3230.

[35] Lu, X., and Gu, X., 2022, A review on lignin pyrolysis: Pyrolytic behavior, mechanism, and relevant upgrading for improving process efficiency, *Biotechnol. Biofuels Bioprod.*, 15 (1), 106.

[36] Saad, M.J., Hua, C.C., Misran, S., Zakaria, S., Sajab, M.S., and Abdul Rahman, M.H., 2020, Rice husk activated carbon with NaOH activation: Physical and chemical properties, *Sains Malays.*, 49 (9), 2261–2267.

[37] Hafizuddin, M.S., Lee, C.L., Chin, K.L., H'ng, P.S., Khoo, P.S., and Rashid, U., 2021, Fabrication of highly microporous structure activated carbon via surface modification with sodium hydroxide, *Polymers*, 13 (22), 3954.

[38] Budianto, A., Kusdarini, E., Effendi, S.S.W., and Aziz, M., 2019, The production of activated carbon from Indonesian mangrove charcoal, *IOP Conf. Ser.: Mater. Sci. Eng.*, 462 (1), 12006.

[39] Jung, H.Y., Gupta, R.K., Oh, E.O., Kim, Y.H., and Whang, C.M., 2005, Vibrational spectroscopic studies of sol–gel derived physical and chemical bonded ORMOSILs, *J. Non-Cryst. Solids*, 351 (5), 372–379.

[40] Thommes, M., Kaneko, K., Neimark, A.V., Olivier, J.P., Rodriguez-Reinoso, F., Rouquerol, J., and Sing, K.S.W., 2015, Physisorption of gases, with special reference to the evaluation of surface area and pore size distribution (IUPAC Technical Report), *Pure Appl. Chem.*, 87 (9-10), 1051–1069.

[41] Tahmasebpoor, M., Iranvandi, M., Heidari, M., Azimi, B., and Pevida, C., 2023, Development of novel waste tea-derived activated carbon promoted with SiO_2 nanoparticles as highly robust and easily

fluidizable sorbent for low-temperature CO_2 capture, *J. Environ. Chem. Eng.*, 11 (5), 110437.

[42] Chouli, F., Ezzat, A.O., Sabantina, L., Benyoucef, A., and Zehhaf, A., 2024, Optimization conditions of malachite green adsorption onto almond shell carbon waste using process design, *Molecules*, 29 (1), 54.

[43] Tran, T.N.D., Tran, T.T., Hoang, B.N., Lam, V.T., and Ngô, T.C.Q., 2024, Synthesis of activated carbon from dragon fruit peel for adsorption of methyl blue, *Indones. J. Chem.*, 24 (6), 1602–1614.

[44] Zhu, D., Li, Q., Honeychurch, K.C., Piano, M., and Chen, G., 2016, Determination of malachite green in aquaculture water by adsorptive stripping voltammetry, *Anal. Lett.*, 49 (9), 1436–1451.

[45] Yi, H., Qu, W., and Huang, W., 2007, Electrochemical determination of malachite green using a multi-wall carbon nanotube modified glassy carbon electrode, *Microchim. Acta,* 160 (1), 291–296.

[46] Singh, H., and Choden, S., 2015, Comparison of adsorption behaviour and kinetic modeling of bio-waste materials using basic dye as adsorbate, *Indian J. Chem. Technol.*, 21, 359–367.

[47] Anbia, M., and Ghaffari, A., 2009, Adsorption of phenolic compounds from aqueous solutions using carbon nanoporous adsorbent coated with polymer, *Appl. Surf. Sci.*, 255 (23), 9487–9492.

[48] Shoushtarian, F., Moghaddam, M.R.A., and Kowsari, E., 2020, Efficient regeneration/reuse of graphene oxide as a nanoadsorbent for removing basic Red 46 from aqueous solutions, *J. Mol. Liq.*, 312, 113386.

[49] Patrulea, V., Negrulescu, A., Mincea, M.M., Pitulice, L.D., Spiridon, O.B., and Ostafe, V., 2013, Optimization of the removal of copper(II) ions from aqueous solution on chitosan and cross-linked chitosan beads, *BioResources*, 8 (1), 1147–1165.

[50] Wahyuhadi, M.E., Kusumadewi, R.A., and Hadisoebroto, R., 2023, Effect of contact time on the adsorption process of activated carbon from banana peel in reducing heavy metal Cd and dyes using a stirring tub (pilot scale), *IOP Conf. Ser.: Earth Environ. Sci.*, 1203 (1), 012035.

[51] Ozcan, D.O., Hendekcï, M.C., and Ovez, B., 2024, Enhancing the adsorption capacity of organic and inorganic pollutants onto impregnated olive stone derived activated carbon, *Heliyon*, 10 (12), e32792.

[52] Oscik, J., and Cooper, I.L., 1992, *Adsorption*, Ellis Horwood Publisher Limited, Chichester, UK.

[53] Hill, T.L., 1946, Statistical mechanics of multimolecular adsorption II. Localized and mobile adsorption and absorption, *J. Chem. Phys.*, 14 (7), 441–453.

[54] Abin-Bazaine, A., Campos Trujillo, A., and Olmos-Marquez, M., 2022, "Adsorption Isotherms: Enlightenment of the Phenomenon of Adsorption" in *Wastewater Treatment*, Eds. Ince, M., and Kaplan Ince, O., IntechOpen, Rijeka, Croatia.

[55] Ragadhita, R., and Nandiyanto, A.B.D., 2022, Curcumin adsorption on zinc imidazole framework-8 particles: Isotherm adsorption using Langmuir, Freundlich, Temkin, and Dubinin-Radushkevich models, *J. Eng. Sci. Technol.*, 17 (2), 1078–1089.

[56] Sogut, E.G., and Caliskan, N., 2017, Isotherm and kinetic studies of Pb(II) adsorption on raw and modified diatomite by using non-linear regression method, *Fresenius Environ. Bull.*, 26 (4), 2721–2729.

[57] Edet, U.A., and Ifelebuegu, A.O., 2020, Kinetics, isotherms, and thermodynamic modeling of the adsorption of phosphates from model wastewater using recycled brick waste, *Processes*, 8 (6), 665.

[58] Karim, M.A., Ahmed, S., Hossain, D., Hossain, M.I.., Hossain, M.S.., Hossain, A., Rahman, M.H., Dipti, S.S., and Azad, M.A.K., 2024, Adsorption isotherms and kinetics studies on adsorption of malachite green onto activated charcoal from aqueous solution, *J. Sci. Eng. Pap.*, 1 (1), 18–25.

[59] Al-Ghouti, M.A., and Da'ana, D.A., 2020, Guidelines for the use and interpretation of adsorption isotherm models: A review, *J. Hazard. Mater.*, 393, 122383.

[60] Wang, J., and Guo, X., 2020, Adsorption kinetic models: Physical meanings, applications, and solving methods, *J. Hazard. Mater.*, 390, 122156.

[61] Yuningsih, N.E., Ariani, L., Suprapto, S., Ulfin, I., Harmami, H., Juwono, H., and Ni'mah, Y.L., 2024,

Adsorption of malachite green using activated carbon from mangosteen peel: Optimization using Box-Behnken design, *J. Renewable Mater.*, 12 (5), 981–992.

[62] Moumen, A., Belhocine, Y., Mechati, F., Karout, M., Charime, D., Boultif, W., and Hattab, Z., 2024, Spectral, isotherm, kinetic, and thermodynamic studies of malachite green dye adsorption from aqueous solutions onto low-cost treated kaolin, *Phys. Chem. Res.*, 12 (1), 47–60.

[63] Pishdadi-Aghdarreh, F., Norouzbeigi, R., and Velayi, E., 2025, KOH-activated lightweight expanded clay aggregate (LECA) for malachite green adsorption: Activation mechanism and adsorption process assessment, *Int. J. Environ. Sci. Technol.*, 22 (7), 5633–5654.

[64] Brunauer, S., Emmett, P.H., and Teller, E., 1938, Adsorption of gases in multimolecular layers, *J. Am. Chem. Soc.*, 60 (2), 309–319.

[65] Saleh, T.A., 2022, Chapter 4 - Isotherm models of adsorption processes on adsorbents and nanoadsorbents, *Interface Sci. Technol.*, 34, 99–126.

[66] Wang, T., Jiang, M., Yu, X., Niu, N., and Chen, L., 2022, Application of lignin adsorbent in wastewater treatment: A review, *Sep. Purif. Technol.*, 302, 122116.

[67] Thakur, A., Assad, H., Kaya, S., and Kumar, A., 2022, "Chapter 17 - Plant extracts as environmentally sustainable corrosion inhibitors II" in *Eco-Friendly Corrosion Inhibitors*, Eds. Guo, L., Verma, C., and Zhang, D., Elsevier, Amsterdam, Netherlands, 283–310,

[68] Dong, Y., Guo, F., Shu, R., Dong, K., Qiao, Q., Liu, S., Xu, L., and Bai, Y., 2022, Evaluation of the high metals-containing coal gasification fine slag as a high-performance adsorbent for malachite green adsorption, *Waste Biomass Valorization*, 13 (12), 4897–4909.

[69] Yadav, V.K., Singh, B., Gacem, A., Yadav, K.K., Gnanamoorthy, G., Alsufyani, T., Hussein, H.S., Awwad, N.S., Verma, R., Inwati, G.K., Swain, K., and Choudhary, N., 2022, Development of novel microcomposite materials from coal fly ash and incense sticks ash waste and their application for remediation of malachite green dye from aqueous solutions, *Water*, 14, 3871.

[70] Ardiyanti, A., Suprapto, S., and Ni'mah, Y.L., 2023, Malachite green adsorption using carbon-based and non-conventional adsorbent made from biowaste and biomass: A review, *J. Renewable Mater.*, 11 (11), 3789–3806.